Aeromonas hydrophila CobQ is a new type of NAD^+- and Zn^{2+}-independent protein lysine deacetylase

Yuqian Wang[1,2]¶, Guibin Wang[1,5]¶, Lishan Zhang[1,3,4], Qilan Cai[1,3,4], Meizhen Lin[1,3,4], Dongping Huang [1,3,4], Yuyue Xie[1,3], Wenxiong Lin[1,3], Xiangmin Lin[1,3,4]*

[1] Fujian Provincial Key Laboratory of Agroecological Processing and Safety Monitoring (School of Life Sciences, Fujian Agriculture and Forestry University), Fuzhou 350002, China

[2] Agricultural College, Anhui Science and Technology University, Chuzhou 233100, China

[3] Key Laboratory of Crop Ecology and Molecular Physiology (Fujian Agriculture and Forestry University), Fujian Province University, Fuzhou 350002, China

[4] Key Laboratory of Marine Biotechnology of Fujian Province, Institute of Oceanology, Fujian Agriculture and Forestry University, Fuzhou 350002, China

[5] State Key Laboratory of Proteomics, Beijing Proteome Research Center, National Center for Protein Sciences (Beijing), Beijing Institute of Lifeomics, Beijing 102206, China

Running title: AhCobQ is a new type of lysine deacetylase

¶ These authors contributed equally to this work.

*Corresponding author: Xiangmin Lin, E-mail: xiangmin@fafu.edu.cn, Agroecological Institute, Fujian Agriculture and Forestry University, Fuzhou 350002, Fujian, PR China. Tel: +86059183769440; Fax: +86059183769440.

Highlights

AhCobQ is an NAD^+- and Zn^{2+}-independent protein lysine deacetylase.

There are no proteins homologous to AhCobQ in eukaryotes.

The deacetylase activity of AhCobQ is located in an unknown domain.

AhCobQ has specific protein substrates and substrates in common with other lysine deacetylases.

AhCobQ positively regulates the enzymatic activity of isocitrate dehydrogenase at its K388 site.

Summary

The lack of exploration of new lysine acetylases and deacetylases (KDACs) and their protein substrates in prokaryotic cells has become a bottleneck in the functional study of lysine acetylation modifications. In this study, we reported a novel Zn^{2+}- and NAD^+-independent KDAC protein, AhCobQ, in *Aeromonas hydrophila*. Interestingly, this protein does not share homology with current known KDACs, and its KDAC activity is located in an unknown domain for which a homologous protein cannot be found in eukaryotic cells. The following analysis showed that AhCobQ affected the enzymatic activity and protein-protein interaction ability of its protein substrates. In summary, these results extended our understanding of the regulatory mechanism of bacterial lysine acetylation modifications.

Abstract

Protein N^{ε}-lysine acetylation (Kac) modifications play crucial roles in diverse physiological and pathological functions in cells. In prokaryotic cells, there are only two types of lysine deacetylases (KDACs) that are Zn^{2+}- or NAD^{+}-dependent. In this study, we reported a protein, AhCobQ, in *Aeromonas hydrophila* ATCC 7966 that presents NAD^{+}- and Zn^{2+}-independent KDAC activity. Furthermore, its KDAC activity is located in an unidentified domain (from 195–245 aa). Interestingly, AhCobQ has no homology with current known KDACs, and no homologous protein was found in eukaryotic cells. A protein substrate analysis showed that AhCobQ has specific protein substrates in common with other known KDACs, indicating that these KDACs can dynamically co-regulate the states of Kac proteins. Microbiological methods employed in this study affirmed AhCobQ's positive regulation of isocitrate dehydrogenase (ICD) enzymatic activity at the K388 site, implicating AhCobQ in the modulation of bacterial enzymatic activities. In summary, our findings present compelling evidence that AhCobQ represents a distinctive type of KDAC with significant roles in bacterial biological functions.

Keywords: Lysine acetylation modification; lysine deacetylases; NAD^{+}/Zn^{2+}-independent; CobQ; *Aeromonas hydrophila*

Introduction

In recent years, due to the development of specific antibody enrichment technologies and high-resolution mass spectrometry, the research on protein post-translational modifications (PTMs) is increasing dramatically, and it provides a new platform for the study of bacterial function and regulation. PTMs refer to small molecular moieties that dynamically affect the structure and function of proteins through chemical modification of specific amino acid residues, so as to regulate many important biological processes, including cell metabolism, DNA transcription and replication, host infection, and stress resistance, and therefore play an important role in almost all physiological functions (Carabetta et al, 2007). Among them, the N^{ε}-lysine acetylation (Kac) modification on protein is widely found in bacteria and participates in almost all key biological processes in bacterial life activities and is attracting the attention of microbiologists (Yu et al, 2023).

Although there are many reports on the identification of acetylation modification patterns of bacterial protein lysine residues in recent years, two fundamental questions have not been solved: how do these acetylation modifications arise (acetylation modifiers; writers) and how are they removed (deacetylation modifiers; erasers) (Wang et al, 2020). On the one hand, acetyl groups can be transferred to the target protein by acetyltransferases or non-enzymatic (chemical) mechanisms (VanDrisse & Escalante-Semerena, 2019); on the other hand, proteins need to remove acetyl groups from modified proteins to reversibly regulate the function of target proteins. At present, the

research on the functions and types of lysine deacetylases (KDACs) has been well documented in eukaryotes, and most of them are histone deacetylases (HDACs). There are currently at least 18 types of HDACs in four classes (I–IV) in mammals and four plant-specific histone deacetylase 2 (HD2) members in plant (Yoshida et al, 2017; Chen et al, 2020). Of these, HDAC types I, II, and IV are Zn^{2+}-dependent, while type III deacetylases are NAD^{+}-dependent sirtuins. Moreover, sirtuins can be divided into seven types (SIRT 1–7), which are distributed in different compartments of eukaryotic cells and perform important biological functions (Narita et al, 2019). Beside these, ABHD14B, a novel KDAC, was reported to deacetylate non-histone substrates and influences glucose metabolism in mammals (Rajendran et al, 2022; Rajendran et al, 2019).

The currently known KDACs in bacteria include Zn^{2+}-dependent RpLdaA or Kdac1 (homologous to eukaryotic type II KDACs), Zn^{2+}-dependent AcuC (homologous to type I), and NAD^{+}-dependent sirtuin (homologous to type III) family proteins (Watson et al, 2023). Sirtuins, represented by *Escherichia coli* CobB, are the most widely distributed KDACs in many bacterial species and are involved in the regulation of a variety of important physiological functions (Burckhardt et al, 2019; Liu et al, 2018; Wang et al, 2020). However, since the first report of the deacetylase function of CobB in *Salmonella typhimurium* in 1998, only two types (three classes) of KDACs have been confirmed in bacteria (Tsang & Escalante-Semerena, 1998; Macek et al, 2019). The reasons that hinder new KDAC discovery in bacteria may be the following: (1) due to the in-depth

109 study of KDACs in eukaryotes, almost all the current research on bacterial
110 deacetylases are based on the characteristics of their homologous proteins in
111 eukaryotes, but less attention is paid to bacteria-specific KDACs; and (2) the
112 deacetylation process between protein substrates and KDACs may be a transient and
113 reversible weak interaction. Moreover, there are thousands of lysine acetylation
114 modification sites in cellular proteins (Chen et al, 2022); so, it is difficult to speculate
115 the characteristics of their specific binding deacetylase, which makes the efficiency of
116 enriching specific KDACs by common protein-protein interaction methods, such as co-
117 immunoprecipitation and pull-down technologies, challenging. As a result, the
118 identification and mechanism of new deacetylases in prokaryotic cells are lagging.
119 Therefore, the screening and identification of new deacetylases, especially for new
120 types of KDACs that may not depend on NAD^+ or Zn^{2+}, have been a bottleneck limiting
121 the research on the regulatory mechanisms of bacterial acetylation/deacetylation
122 modifications.
123
124 In this study, we fortuitously identified the protein AhCobQ in *Aeromonas hydrophila*
125 ATCC 7966 (UniProt ID A0KI27, gene ID *AHA_1389*) that presents NAD^+- and Zn^{2+}-
126 independent protein lysine deacetylase activity. Interestingly, although this protein is
127 described as a CobQ/CobB/MinD/ParA family protein in the UniProt database, it is
128 homologous with cobyric acid synthase in other bacterial species but shares no
129 homology with CobB sirtuin family proteins. In addition to deacetylating lysine
130 acetylated sites common to AhCobB (UniProt ID A0KKN9, gene ID *AHA_2317*) sirtuin

131 and another deacetylase AhAcuC (UniProt ID A0KLZ2, gene ID *AHA_2788*) in *A.*
132 *hydrophila*, we also confirmed that AhCobQ deacetylated specific lysine acetylated
133 sites as did other KDACs, even in the same protein. In general, our results
134 demonstrated a new type of bacterial KDAC, which shares no homology with currently
135 known lysine deacetylases, including those in eukaryotic cells, and extends our
136 understanding of the complicated regulatory mechanism of bacterial lysine acetylation
137 modifications.
138

139 ## Results

140 ***The physiological phenotypes of AhCobQ are different from those of AhCobB***

141 This project proceeded from the misunderstanding that AhCobQ and AhCobB may be
142 homologous proteins because AhCobQ is annotated as a CobQ/CobB/MinD/ParA
143 family protein in the UniProt database. Therefore, we constructed *ahcobB* and *ahcobQ*
144 mutant strains (**Figure 1A**) and compared their general physiological phenotypes.
145 When compared to the wild-type strain (WT), the deletion of *ahcobB* did not affect the
146 hemolytic or swarming ability of *A. hydrophila*. Notably, *⊿ahcobQ* did not affect the
147 hemolytic ability either but significantly increased the swarming ability (**Figure 1B , C**
148 **and Figure S1**). Most interestingly, *⊿ahcobB* sharply increased, while *⊿ahcobQ*
149 significantly decreased, the bacterial biofilm formation ability (**Figure 1D**). These
150 results indicated that CobB and CobQ in *A. hydrophila* may play different roles in
151 biological functions.
152

153

154 ***AhCobQ and AhCobB are not homologous proteins***

155 We then further investigated the evolutionary relationship between AhCobQ and
156 AhCobB. To our surprise, we found that the proteins belong to different protein families.
157 AhCobB (UniProt ID A0KKN9) belongs to a well-known NAD^+-dependent protein
158 deacylase sirtuin family and shares a highly homologous SIR2 domain with CobB
159 sirtuins in many bacterial species, such as *E. coli* (NPD_ECOLI), *S. typhimurium*
160 (NPD_SALTY), *Pseudomonas nitroreducens* (A0A246F352_9PSED), and even seven
161 types of sirtuins in humans (**Figure 2A**). However, AhCobQ (UniProt ID A0KI27) shares
162 an AAA_31 ATPase domain with several homologous proteins, such as cobalamin
163 biosynthesis protein CobQ in *P. nitroreducens* (A0A246FC44_9PSED), probable
164 plasmid partitioning protein in *P. aeruginosa* (G3XCW7_PSEAE), and chromosome
165 partitioning ATPase in *S. typhimurium* (A0A0F6B556_SALT1). Moreover, AhCobQ also
166 shares homology with Soj protein (A0KQY7_AERHH) and cell division inhibitor MinD
167 (A0KK56_AERHH) in *A. hydrophila* as well (**Figure 2B and Figure S2**). Interestingly,
168 this protein was not found to have homologous proteins in humans or mice species,
169 indicating the significant evolutionary difference between AhCobQ and sirtuins.

170

171 ***AhCobQ is an NAD- and Zn^{2+}-independent lysine deacetylase***

172 Dot blot and western blot experiments showed that the deletion of *ahcobQ* or *ahcobB*
173 both significantly increased the whole protein lysine acetylation levels in *A. hydrophila*
174 cells (**Figure 2C and D**), which aroused our interest as to whether AhCobQ is a lysine

175 deacetylase or not. To test this possibility, we purified AhCobQ, AhAcuC, and AhCobB
176 proteins and incubated them *in vitro* with lysine acetylated-bovine serum albumin (Kac-
177 BSA) as a protein substrate with and without NAD^+ or Zn^{2+} treatment (**Figure S3 and**
178 **S4**). As a positive control, AhCobB and AhAcuC significantly deacetylated Kac-BSA in
179 the presence of NAD+ or Zn2+ buffer, which met our expectation. However, AhCobQ
180 clearly deacetylated Kac-BSA regardless of whether NAD^+ or $Zn2^+$ were present
181 (**Figure 2E and G**). Moreover, the KDAC activity of AhCobB was inhibited when the
182 sirtuin inhibitor nicotinamide (NAM) was added, but this did not affect the deacetylase
183 activity of AhCobQ (**Figure 2F**). Furthermore, the introduction of the metal ion chelator,
184 EDTA, had no discernible effect on the deacetylase activity of AhCobQ (**Figure S5**).
185 These results strongly indicate that AhCobQ is an NAD^+- and Zn^{2+}-independent protein
186 deacetylase. Additionally, since AhCobQ has an ATPase domain at the N-terminal, we
187 also tested its deacetylase activity with or without ATP (**Figure 2H and Figure S6**).
188 The results demonstrated that the KDAC activity of AhCobQ was ATP-independent,
189 suggesting its enzymatic activity was downstream of the ATPase domain.
190
191 We further digested Kac-BSA to peptides after AhCobQ incubation and then subjected
192 the peptides to LC MS/MS to identify their acetylated sites (**Table S1**). The results
193 showed that the MS intensities of at least 15 Kac peptides in BSA were significantly
194 decreased after AhCobQ treatment. To further validate the KDAC characteristics of
195 AhCobQ and exclude the possibility that AhCobQ may hydrolyze Kac peptides or
196 switch the lysine acetylation to other unknown PTMs, we selected and synthetized an

197 acetylated peptide sequence (YNGVFQECCQAEDK^{ac}GACLLPK) with its unacetylated
198 peptide as negative control and subjected them to additional deacetylation assays. The
199 synthetized acetylated (STD*^{Kac}) and deacetylated (STD) peptides were incubated with
200 AhCobB and AhCobQ and then identified by LC MS/MS. As shown in **Figure 3**, the
201 masses of the STD*^{Kac} and STD peptides were 786.35538 (3+) and 772.35175 (3+),
202 respectively. When the STD*^{Kac} peptide was incubated with AhCobB or AhCobQ, the
203 corresponding retention time in the C18 chromatography and the MS1 peak of the
204 deacetylated peptide were found in both treatments **(Figure 3A and B)**. Moreover, the
205 deacetylated and acetylated peptides were further validated in MS2 by LC MS/MS
206 **(Figure 3C and D)**. These results indicate that AhCobQ is not a hydrolase that
207 hydrolyzes target proteins but likely a protein deacetylase similar to AhCobB.
208
209 ***The deacetylase activity of AhCobQ is in an unidentified domain***
210 Because AhCobQ has a conservative N-terminal AAA family ATPase domain (1–179
211 aa) and its KDAC activity was not affected by ATP, we then asked whether this domain
212 has deacetylase activity. We divided and purified recombinant AhCobQ protein into two
213 truncated protein fragments of 1–179 aa and 179–264 aa and then tested their
214 deacetylase activities. To our surprise, the 179-264 aa protein fragment but not the 1-
215 179 aa fragment showed NAD^+- and Zn^{2+}-independent deacetylase activity (**Figure**
216 **4A**). To better understand the deacetylase domain of AhCobQ, a total of 12 truncated
217 protein fragments were constructed and purified, and their deacetylase activities were
218 evaluated (**Figures S7 and 4A**). As shown in **Figure 4**, the 1–179 aa, 200–255 aa,

219 and 189–240 aa shortened proteins disrupted the deacetylase activity of AhCobQ to
220 some extent, whereas the 179–264 aa, 189–264 aa, 199–264 aa, 195–264 aa, 195–
221 255 aa, 189–245 aa, 189–250 aa, 189–255 aa, and 189–264 aa shortened proteins
222 did not, indicating that the deacetylase activity may be in the 195–245 aa range.
223 Interestingly, although the full amino acid sequence of AhCobQ (1–254 aa) is
224 homologous with Soj protein (A0KQYT), site-determining protein (A0KI19 and
225 A0KK56), and ParA family protein (A0KQG8) in *A. hydrophila*, the KDAC activity
226 domain (195–245 aa) does not share homology with these proteins, which suggests
227 the different biological roles among them. Moreover, AhCobQ (195–245 aa) also
228 shares homology with several prokaryotic species, such as *Aeromonas sp., Aliivibrio*
229 *sp., Enterovibri sp., Oceanimonas sp., Photobacterium sp.,* and *Vibrio sp*., most of
230 which are marine prokaryotes based on a PSI-BLAST program searching, but the
231 search failed to find homologous proteins in eukaryotic cells (**Figure 5**). Therefore, the
232 195–245 aa shortened protein of AhCobQ may represent a new domain that exhibits
233 NAD^+- and Zn^{2+}-independent deacetylase activity.
234

235 ***AhCobQ, AhCobB, and AhAcuC deacetylate different acetylated proteins and***
236 ***sites***

237 We then identified the proteins that were substrates of AhCobQ and analyzed the
238 substrate differences among AhCobQ, AhCobB, and a predicted Zn^{2+}-dependent
239 deacetylase AhAcuC of *A. hydrophila* that is homologous to type I KDACs in
240 eukaryotes. A quantitative lysine acetylome was generated to compare the differential

241 expression of lysine acetylated peptides among *ahcobQ*, *ahcobB*, and *ahacuC* gene-
242 deficient strains and their WT strain (**Figure 6, Figures S8-S110 and Table S2**). We
243 only focused on the upregulated lysine acetylated peptides between the mutant and
244 WT strains. When compared to WT, the deletion of *ahcobQ*, *ahcobB*, and *ahacuC* led
245 to increased abundances at 52 Kac sites (corresponding to 47 Kac proteins), 370 Kac
246 sites (291 proteins), and 197 Kac sites (176 proteins), respectively. Moreover, there
247 were 19 increased Kac peptides common between the Δ*ahcobQ* and Δ*ahacuC*
248 strains, 10 increased Kac peptides common between the Δ*ahcobQ* and Δ*ahcobB*
249 strains, 69 increased Kac peptides common between the Δ*ahcobB* and Δ*ahacuC*
250 strains, and four peptides common among the Δ*ahcobQ*, Δ*ahcobB*, and Δ*ahacuC*
251 strains (**Figure 6A**). We also found that there were only 531 Kac peptides directly
252 regulated by these three deacetylases, which is only a small proportion of the total Kac
253 peptides (accounting for 10.28% of all 3,163 Kac peptides identified in the current
254 study), indicating the presence of other unknown KDACs in this bacterium.
255
256 A KEGG pathway analysis showed that biosynthesis of amino acids and antibiotics
257 was enriched in the unique upregulated Kac proteins in the Δ*ahcobQ* strain (**Figure**
258 **6B**). Furthermore, five pathways, namely, pyrimidine metabolism, metabolic pathways,
259 purine metabolism, pyruvate metabolism, and RNA polymerase, were enriched in
260 upregulated Kac proteins under AhCobB-regulation. Of these three deacetylase
261 mutants, Δ*ahacuC* enriched the most metabolic pathways, although Δ*ahcobB*
262 regulated more Kac sites. Carbon metabolism, biosynthesis of antibiotics, and

263 glycolysis/gluconeogenesis pathways were the top three enrichment pathways in the
264 unique 119 Kac sites regulated by AhAcuC. Phosphotransferase system (PTS),
265 microbial metabolism in diverse environments, and metabolic pathways were enriched
266 in the upregulated Kac proteins common to the Δ*ahacuC* and Δ*ahcobB* mutants. In
267 general, although there are different pathways involved in the activity of different
268 deacetylases, most of the Kac proteins regulated by these KDACs were enzymes and
269 normally had important roles in metabolic pathways.
270
271 ***Validation of the specificity of Kac proteins and sites by deacetylases***
272 We further validated the specificity of Kac proteins and the sites regulated by these
273 deacetylases. A total of 11 target proteins (HrpA, SUN, ENO, ArcA, ADK, IscS, A0KJ75,
274 GyrB, FtsA, RecA, and ICD) were selected for validation due to their significantly
275 upregulated Kac levels in the *ΔahcobQ* strain, potentially indicating their roles as
276 substrates for AhCobQ. These proteins were first cloned and purified in *E. coli*. The
277 anti-Kac western blot showed that these purified proteins did not have lysine
278 acetylation signals, which may be because of the heterologous expression in an
279 engineered bacterial strain. This was ideal for excluding signal interference from the
280 background (**Figure S11**). Next, site-specific lysine acetylation of the target protein
281 substrates was constructed using a two-plasmid-based system of genetically encoded
282 N^{ε}-acetyllysine, which was purified and incubated with AhCobQ, AhCobB, and AhAcuC
283 for western blot analysis against anti-lysine acetylation antibodies (**Figure S12**). As
284 shown in **Figure 7A**, when compared to untreated Kac proteins, the acetylation level

285 of four Kac sites (K816 in HrpA, K103 and K148 in SUN, K195 in ENO) that were
286 uniquely regulated by AhCobQ according to quantitative acetylome analysis was
287 significantly reduced after incubation with AhcobQ but unchanged after incubation with
288 AhCobB or AhAcuC. Moreover, K26 in ArcA-2 and K48 in ADK were reduced in both
289 AhCobB and AhCobQ incubations, and K93 in IscS and K81 in A0KJ75 were
290 decreased with all three deacetylases (**Figure 7A**). These results were consistent with
291 our quantitative acetylome results, except for K34 in GlmM, which was decreased in
292 AhCobB and AhCobQ treatments in the western blotting assay but upregulated by all
293 three deacetylase mutants according to the proteomics data (**Figure S13**). Intriguingly,
294 several proteins that contained multiple Kac sites were found to be regulated by
295 different deacetylases. For example, K331 and K449 in GyrB were deacetylated by
296 AhCobQ and AhCobB, respectively (**Figure 7B**). The same results were found in K320
297 and K409 in FtsA and in K279 and K306 in RecA as well. These results indicate the
298 different regulatory mechanisms among these KDACs.
299
300 ***AhCobQ positively regulates the enzymatic activity of isocitrate dehydrogenase***
301 ***(ICD) at K388 site***
302 To further understand the effect of AhCobQ on bacterial biological function, an AhCobQ
303 substrate, *A. hydrophila* isocitrate dehydrogenase (ICD) was cloned and purified in *E.*
304 *coli*（**Figure S12**）. Western blot assay showed that this protein didn't display lysine
305 acetylation modification in *E. coli* (**Figure 8A**). Therefore, site-specific lysine
306 acetylation was constructed at K388 site of ICD for further enzymatic activity

307 determination. As showed in **Figure 8B**, AhCobQ can significantly deacetylated ICD at
308 K388, while other two deacetylases, AhCobB and AhAcuC didn't. This result is
309 consistent with the proteomics conclusions. When compared with unKac ICD protein,
310 the Kac at K388 of ICD significantly decreased the product of NADPH with the adding
311 of $NADP^+$ substrate, which indicate the Kac at K388 negatively regulates the enzymatic
312 activity of ICD. Moreover, the adding of AhCobQ significantly increased the enzymatic
313 activity of K388 acetylated ICD and quickly reached the platform period in 10 minutes,
314 while AhCobB and AhAcuC didn't affect ICD enzymatic activity (**Figure 8C and D**).
315 These results indicate that AhCobQ positively regulates the enzymatic activity of
316 isocitrate dehydrogenase by deacetylating the ICD protein at K388 site.
317

318 ## Discussion

319 Lysine acetylation has been confirmed to play crucial roles in almost all essential
320 biological functions in both eukaryotic and prokaryotic cells. Normally, reversibility and
321 dynamicity are necessary characteristics of lysine acetylation. The regulatory
322 mechanism of deacetylation has received as much attention as that of acetylation. In
323 different bacterial species, there are hundreds to thousands of protein lysine
324 acetylation modification sites, which are theoretically unlikely to be regulated by one
325 or a few deacetylases, and there must be some unknown deacetylases in bacteria that
326 act on specific protein substrates to maintain the normal physiological function of cells.
327 Therefore, finding new bacterial deacetylases and identifying their modified protein
328 substrates, so as to better understand the molecular mechanism of their regulation,

329 are important in the research on protein acetylation modification regulation.

330

331 Here, we reported that CobQ protein in *A. hydrophila* is an NAD^+- and Zn^{2+}-
332 independent deacetylase, and it is very different from currently known deacetylases.
333 We were first interested in the function of AhCobQ based on its annotation as a
334 CobQ/CobB/MinD/ParA family protein in the UniProt database. The deacetylation
335 assay suggested that AhCobQ deacetylated Kac-BSA in the same manner as AhCobB.
336 To our surprise, AhCobQ does not share homology with any prokaryotic sirtuin CobB
337 or currently known eukaryotic deacetylases. We then asked why this was the case
338 since both proteins appeared to belong to the same protein family. Actually, CobB has
339 a conflicting naming phenomenon in the UniProt annotation. There are two distinct
340 CobB annotations in the UniProt database: one is the well-known NAD-dependent
341 protein deacylase, such as NPD_ECOLI in *E. coli*, and the other is the ATP-dependent
342 a,c-diamide synthase, such as CobB_SINSX *in Sinorhizobium sp.* that plays an
343 important role in cobalamin biosynthesis (Galperin & Grishin, 2000). In some bacterial
344 species, a,c-diamide synthase is also annotated as CbiA (such as CBIA_SALTY, for
345 example), indicating the controversial assignment of CobB. Interestingly, there is not
346 an a,c-diamide synthase homologous protein in *A. hydrophila* ATCC 7966, and the
347 CobB annotation in *A. hydrophila* ATCC 7966 is specific for NAD-dependent protein
348 deacylase. In general, the CobQ protein is annotated as cobyric acid synthase and
349 belongs to a,c-diamide synthase (CobB or CbiA) but not the sirtuin protein (CobB)
350 family. The role of AhCobQ is unknown to date because *A. hydrophila* may import
351 rather than synthesize cobalamin (vitamin B12) (Seshadri et al, 2006).

352

353 The LC MS/MS analysis of synthesized Kac peptides treated by AhCobQ further
354 validated that this protein is a deacetylase and excluded the possibility of it being a
355 hydrolase. Surprisingly, the enzymatic activity of AhCobB was not affected by NAD^+,
356 Zn^{2+}, or the sirtuin inhibitor NAM. Given that AhCobQ was reported to be an ATP-
357 dependent cobyric acid synthase (Galperin & Grishin, 2000), we also tested the effect
358 of ATP on deacetylase activity but obtained negative results. Thus, the deacetylase
359 activity of AhCobQ was determined to be NAD^+-, Zn^{2+}-, and ATP-independent.
360 Subsequent assays showed that the deacetylase activity of AhCobQ was mediated by
361 an unknown C-terminal domain in the 195–245 aa range that was downstream of the
362 predicted ATPase domain, suggesting a new domain was responsible for deacetylation.
363 However, the intrinsic enzymatic mechanism needs to be further investigated.

364

365 We then further asked whether the protein substrates of AhCobQ were the same as
366 the unknown bacterial KDAC homologs in *A. hydrophila*, AhCobB, and AhAcuC.
367 Although the CobB substrates were identified in *E. coli*, the AcuC substrates and their
368 comparison with the CobB substrates at a high throughput level had not been
369 determined (Kuhn et al, 2014; Weinert et al, 2017). The characteristics of Kac sites
370 regulated by CobB and AcuC are not yet known. Here, we compared the differential
371 expression of Kac proteins and sites among *ahcobQ*, *ahcobB*, and *ahacuC* mutant and
372 wild-type strains using a quantitative proteomics method. We only focused on the high
373 abundance Kac proteins or sites (fold change > 1.5) when comparing the mutant and

374 WT strains. The results showed that 9.9% of the acetylated proteins (312/3164 Kac
375 protein) were regulated by *ahcobB*, which is consistent with the proportion in the *E.coli*
376 *cobB* mutant and the previous conclusion that CobB is the predominate deacetylase
377 in some bacterial species (Weinert et al, 2013; AbouElfetouh et al, 2015). We also found
378 47 and 186 significantly enriched Kac proteins in *⊿ahcobQ* and *⊿ahacuC*, respectively.
379 Interestingly, there were unique and overlapping Kac substrates among three KDACs,
380 indicating that these KDACs may construct a complicated network for co-regulation of
381 acetylation proteins. Furthermore, although the enriched GO terms and related
382 substrates were different, all the KDACs appeared to be involved in metabolic
383 pathways.
384
385 To further validate our proteomics results, plasmid-based site-specific acetylation was
386 introduced as a target of the recombinant proteins, and the deacetylase activity of the
387 KDACs was determined *in vitro*. The behavior of the three KDACs on a total of 14
388 target site-specific acetylated proteins was consistent with our proteomics results, with
389 the results exceeding our expectations. AhCobQ regulated certain proteins at specific
390 Kac sites, which implied that it is involved in specific biological functions. Moreover, it
391 also co-regulated the same Kac sites as did one or all the other KDACs, indicating that
392 the cooperation of these KDACs may play an important role during the maintenance
393 of cellular acetylation homeostasis. Most importantly, our results also showed that
394 AhCobQ deacetylated different Kac sites on the same protein as AhCobB or AhAcuC.
395 For example, the bacterial topoisomerases DNA gyrase GyrB is an essential enzyme

396 that controls the topological state of DNA during replication (Tari et al, 2013). Previous
397 studies reported the important role of GyrB in bacterial fluoroquinolone resistance
398 (Chauffour et al, 2021; Li et al, 2022). The 3D structure prediction showed that GyrB
399 K331 is located in the ATPase domain that is responsible for supercoiling DNA,
400 whereas K449 is located in the Toprim domain that is required for the interaction with
401 GyrA (Brino et al, 2000). Our current data showed that K331 and K449 were
402 deacetylated by AhCobQ and AhCobB, respectively, indicating the delicate regulatory
403 mechanisms in both functional domains. To our knowledge, this is the first evidence
404 that different KDACs regulate the Kac level at specific sites of the same protein and
405 that they may be involved in differential biological functions in prokaryotic cells. To our
406 knowledge, it is the first evidence that different KADCs regulates the Kac level at
407 specific-site of one protein and that may involve in differential biological functions in
408 prokaryotic cell. We then further wondered the role of AhCobQ in bacterial biological
409 functions. Isocitrate dehydrogenase (ICD) is a key enzyme in the tricarboxylic acid
410 cycle pathway, and also affects bacterial biofilm formation and virulence in several
411 species. Diverse Kac sites of bacterial ICD have been well identified. In *E. coli* K12,
412 there are at least 15 Kac sites on ICD , and the Kac at K55 and K350 have been
413 determined to play crucial roles on the enzymatic activity by a positively regulatory
414 manner, while Kac at K100, K230 and K235 in a negatively regulatory manner .
415 However, only four Kac sites including K55, K142, K177 and K350 have been proved
416 to be deacetylated by CobB sirtuin obviously. In our quantitative MS data, there are at
417 least ten Kac sites in ICD protein, while only the Kac level of ICD K388 was AhCobQ

418 regulated and others were not altered in KADCs deleted strains. The following assay
419 confirmed that the enzymatic activity of ICD was negatively regulated in a dose-
420 dependent manner by deaectylated ICD K388 site by AhCobQ, whereas not affected
421 by AhCobB and AhAcuC. These results indicate the important role of AhCobQ in
422 bacterial metabolic regulation.
423

424 Conclusion

425 In summary, here, we identified a novel NAD^+- and Zn^{2+}-independent deacetylase,
426 AhCobQ, in prokaryotic cells, which does not share homology with current known
427 deacetylases and is unique in prokaryotes. The deacetylase activity of this KDAC is
428 through an unknown domain. Moreover, AhCobQ acetylates at least 47 protein
429 substrates involved in many biological processes, especially metabolic pathways. We
430 provide evidences that AhCobQ negatively regulates the enzymatic activity of bacterial
431 isocitrate dehydrogenase at K388 site. These results indicate that AhCobQ has an
432 important regulatory role in bacterial metabolic pathways. AhCobQ is a novel
433 deacetylase in prokaryotic cells and its biological functions need to be further
434 investigated.
435

436 Chemicals and reagents

437 Ni-NTA agarose beads were purchased from Yeasen Biotechnology; C18 ZipTips from
438 Millipore Corporation; water and acetonitrile from Thermo Fisher Scientific; and formic
439 acid (FA), dithiothreitol, acetone, and iodoacetamide from Sigma Aldrich. Synthesized

440 peptides were purchased from Science Peptide (Shanghai, China) with 95–99% purity.
441 All chemicals and reagents used in this study are listed in **Table S3**. Critical commercial
442 assay kits used in this study are listed in **Table S4**.
443
444
445 # Methods
446 **Bacterial strains and growth conditions**
447 All strains and vectors involved in this study were preserved or constructed in our
448 laboratory; these are listed in **Table S5**. *A. hydrophila* was cultured at 30°C, and *E. coli*
449 was cultured at 37°C. All bacterial solutions were transferred at 1:100 (v:v; bacterial
450 solution : LB) and cultured continuously for 16 h at 200 rpm, unless otherwise specified.
451
452 **Generation of gene-deleted strains**
453 According to the whole genome sequence of the *A. hydrophila* ATCC 7966 strain,
454 upstream and downstream fragments of the target gene of about 500 bp were amplified.
455 The amplified gene fragments were ligated with the digested pRE112 plasmid using
456 the restriction sites *SacI* and *XbaI* and then transformed first into *E. coli* MC1061. The
457 plasmid was collected and transformed into *E. coli* S17 and then introduced into *A.*
458 *hydrophila* by bacterial conjugation. The positive clones were selected on resistant LB
459 plates (100 μg/mL ampicillin and 30 μg/mL chloramphenicol). Finally, the positive
460 mutants from the previous step were spread on LB plates containing 20% sucrose,
461 and a single clone was picked. The positive result was sent to Shanghai Sangon

462 Biological Co., Ltd. for sequencing, and the bacteria were kept at −80°C for later use
463 (Li et al, 2019; Kou et al, 2022).
464
465 **Physiological phenotype assay**
466 The physiological phenotyping was performed as previously described (Li et al, 2019;
467 Cai et al, 2019). Briefly, for hemolytic and swarming motility assays, bacteria cultured
468 overnight were spotted on 0.7% sheep blood or 0.4% agar plates, respectively, at 30°C
469 for 16 h, and the diameter of the hemolytic or swarming circle was observed and
470 measured in three independent experiments. The bacterial biofilm formation ability was
471 measured with a SpectraMax® i3 multifunctional microplate reader using the crystal
472 violet staining method, and the absorbance at an optical density (OD) of 595 nm
473 wavelength was measured, as previously described (Li et al, 2019). All these
474 experiments were independently repeated three times, and the one-way ANOVA
475 method was used for statistical analysis.
476
477 **BSA acetylation *in vitro***
478 Briefly, 1 mg of BSA powder was dissolved in 1 mL of ddH_2O containing 0.1 M Na_2CO_3
479 and 0.04 g of acetic anhydride and then incubated at 37°C to react for 3 h to produce
480 Kac-BSA. Finally, 20 μL of 1 M Tris (pH 8.0) was added to stop the reaction (Guan et
481 al, 2010).
482
483 **Protein deacetylation assay *in vitro***

484 Briefly, 1 μg of protein or peptides were mixed with 0.2 μg of purified KDAC protein in
485 basic buffer (150 mM Tris-HCl, pH 8.0, and 10% glycerol) with 10 mM $ZnCl_2$, 0.5 mM
486 ATP, 0.25 mM NAD^+, or 0.5 mM NAM, as appropriate, and then incubated at 37°C for
487 3 h (Li et al., 2024).
488
489 **Quantitative acetylome analysis**
490 The quantitative acetylome was performed as previously described (Zhang et al, 2022).
491 Briefly, the protein samples from bacteria cultured overnight were collected by
492 centrifugation and then sonicated in an ice bath. A 10 mg protein sample was reduced
493 by 10 mM dithiothreitol (DTT), alkylated by 20 mM iodoacetamide (IAA), and then
494 digested to peptides by trypsin at a 1:50 ratio at 37°C for 16 h. The lysine acetylation
495 peptides were enriched by an immuno-affinity enrichment method using an agarose-
496 conjugated anti-lysine-acetylated antibody (Hangzhou Jingjie, PTM 101).
497
498 **LC MS/MS**
499 For BSA acetylation identification, the digested peptides were analyzed on an Orbitrap
500 Q Exactive HF mass spectrometer (Thermo Fisher Scientific) equipped with an EASY-
501 nLC 1200 system (Thermo Fisher Scientific). The peptides were first loaded into a C18
502 trap column (1.9 μm, 100 μm, 20 mm) and separated on an EASY-nLC 1200 UPLC
503 system. The precursor ions were selected for fragmentation in the higher energy
504 collision-activated dissociation (HCD) cell at a normalized collision energy of 27% and
505 then detected using the Orbitrap analyzer at a resolution of 15,000 at m/z 200.

506

507 The synthetic peptides YNGVFQECCQAEDKGACLLPK (STD) and YNGVFQECCQA
508 EDK^{ac}GACLLPK (STD^{*Kac}) were analyzed using an Orbitrap Fusion mass spectrometer
509 (Thermo Fisher Scientific) equipped with an EASY-nLC 1200 system (Thermo Fisher
510 Scientific). For the quantitative acetylome, the enriched peptides were analyzed using
511 an Orbitrap Exploris 480 mass spectrometer equipped with a high-field asymmetric
512 waveform ion mobility (FAIMS) Pro spectrometer and an EASY-nLC 1200 system
513 (Thermo Fisher Scientific).

514

515 The data obtained were compared and annotated with the BSA (UniProt ID P02769)
516 or *A. hydrophila* ATCC 7966 database from the UniProt database using MaxQuant
517 v1.6.2.10 software. The mass error of the search was set to 10 ppm, the main search
518 was set to 5 ppm, the fragment ion was set to 0.02 Da, and the variable modification
519 was acetylation modification. The maximum false discovery rate (FDR) threshold for
520 proteins, peptides, and modification sites was set at 1%. In addition, the localization
521 probability threshold was specified as >0.75, and the modification site score threshold
522 was set to 40. The precursor area for quantification of synthetic peptides
523 YNGVFQECCQAEDKGACLLPK (STD) and YNGVFQECCQAEDK^{ac}GACLLPK
524 (STD^{*Kac}) was manually exacted with Thermo Xcalibur (v.3.0.63). When performing a
525 label-free quantitative (LFQ) comparison, in addition to the above settings, label-free
526 quantification was also set to LFQ, and the intensity signal ratio of the corresponding
527 modified peptides in the identification results (ratio) was >1.5. P<0.05 (Student's *t* test)

528 among the three biological replicates in each group was considered a significant
529 difference.
530
531 **Western blot**
532 The protein samples (0.2 μg) were separated on a 12% sodium dodecyl-sulfate
533 polyacrylamide gel electrophoresis (SDS-PAGE) gel and then transferred to
534 polyvinylidene fluoride (PVDF) membranes using a semi-dry transfer system (Bio-Rad,
535 USA) at 25 V for 20 min. The membranes were blocked with Tris-buffered saline with
536 0.1% Tween 20 (TBST) containing 5% skim milk for 1 h and incubated with the diluted
537 primary antibody (PTM-101 1:1,000) for 5 h at room temperature. After washing three
538 times with TBST, the membranes were incubated with the secondary antibody,
539 horseradish peroxidase-conjugated goat anti-mouse IgG (1:5,000), at room
540 temperature for 1 h. Finally, the membranes were covered with Clarity western ECL
541 (Bio-Rad) chromogenic solution and exposed with a ChemiDoc MP (Bio-Rad, Hercules,
542 CA, USA). The exposed PVDF membranes were stained with Coomassie R-350 to
543 verify whether the loading amounts were consistent (Peng et al, 2019).
544
545 **Dot blot**
546 10 μg protein was diluted and spotted on the PVDF membrane. Once the samples had
547 air-dried, the membranes underwent a blocking process with Tris-buffered saline with
548 Tween 20 (TBST) containing 5% BSA for a duration of 3 to 5 hours. Following this,
549 they were incubated with the PTM-101 antibody at a 1:1000 dilution for 5 hours.

550 Afterward, the membranes were washed three times in TBST, then incubated with a
551 secondary antibody, goat anti-mouse HRP-IgG, at a 1:5000 dilution and containing 3%
552 BSA, for one hour at room temperature. This was followed by five washes in TBST,
553 each lasting 5 minutes. To conclude the process, the membrane was treated with
554 Clarity Western ECL Substrate (Bio-Rad) chromogenic solution, exposed using a
555 ChemiDoc MP imaging system (Bio-Rad, Hercules, CA, USA), and finally stained with
556 Coomassie R-350 to ensure consistent sample loading.
557
558 **Recombinant protein production and purification**
559 The target genes were amplified and ligated to the digested pET-21b/32a plasmid
560 using the restriction sites *EcoRI* and *HindIII*. Then, the recombinant plasmid was
561 transformed into competent *E. coli* BL21 (DE3), and the positive clones were selected
562 from an agar plate with 100 μg/mL ampicillin. For the construction of site-directed
563 mutant strains, the target gene was mutated using a Fast Mutagenesis System kit
564 according to the manufacturer's protocol (Transgen Biotech Co., Beijing, China). All
565 primer pairs used in this study are listed in **Table S6**.
566
567 The successfully constructed recombinant strains were transferred to 200 mL of LB
568 medium containing 100 μg/mL ampicillin, and then, 200 μL of 1 M isopropyl β-D-1-
569 thiogalactopyranoside (IPTG) was added until the OD at 600 nm reached about 0.6.
570 After washing three times with phosphate-buffered saline (PBS) and dissolving in 10
571 mL of a solution (5 mM imidazole, 0.5 mM NaCl, 0.05M Tris-HCl pH=8.0), the bacterial

572 cells were ultrasonically disrupted for 20 min on ice. The supernatant was collected by
573 centrifuging at 10,000 rpm at 4°C for 15 min, and the recombinant proteins were
574 purified using an Ni^{+}-NTA column as previously described (Jiang et al, 2022).
575
576 **Expression and purification of site-specific Kac proteins**
577 We used two genetic code expansion systems in *E. coli* BL21 to express site-specific
578 acetylated proteins (Vidali G et al, 1968; Bryson et al, 2017). First, the target gene was
579 inserted into the pET-21b plasmid as described above, and the lysine codon at the
580 target position of the gene was substituted with an amber stop (TAG) codon by site-
581 directed mutagenesis. Then, equal amounts of pTECH-MbAcK3RS (IPYE) and
582 recombinant pET-21b plasmid were co-transfected into competent *E. coli* BL21 (DE3)
583 on agar plates containing 100 μg/mL ampicillin and 30 μg/mL chloramphenicol. After
584 culturing for 5 h at 37°C and 200 rpm, the successful PCR products were confirmed
585 with DNA sequencing.
586
587 The successfully site-specific acetylated mutants were cultured overnight in 5 mL of
588 LB medium and then transferred to 200 mL of fresh LB medium containing 100 μg/mL
589 ampicillin and 30 μg/mL chloramphenicol and incubated at 200 rpm and 37°C. To
590 express the acetyl proteins, 2 mM N-acetyllysine and 20 mM NAM were added to the
591 medium at 37°C and vortexed at 200 rpm until the OD at 600 nm reached about 0.8.
592 Then, 200 μL of 1M IPTG was added to the medium, and the cells were cultured at
593 16°C and vortexed at 200 rpm for 18 h to express the proteins. The procedure of site-

594 specific Kac protein purification was the same as the method described above.

595

596 **Bioinformatics and data analysis**

597 Amino acid sequences were obtained from the UniProt database
598 (https://www.uniprot.org/uniprot). The pfam database (https://www.pfam.org/) was
599 used to predict protein domains, and the online software iTOL (https://itol.embl.de/)
600 was used to generate graphs. The amino acid sequence homology analysis was
601 carried out using position-specific iterated BLAST (PSI-BLAST) software after two
602 iterations (https://blast.ncbi.nlm.nih.gov/Blast.cgi). MEGA v7.0.26 software was used
603 to construct the evolutionary tree that was visualized by online Chiplot software
604 (https://www.chiplot.online/). The protein 3D structure was predicted by AlphaFold in
605 the UniProt database and was visualized by PyMMOL v.2.5.2. The online software
606 STRING v.11.5 (http://string-db.org/) was used to perform Kyoto Encyclopedia of
607 Genes and Genomes (KEGG) metabolic pathway enrichment analysis for upregulated
608 proteins, and these proteins were finally visualized using Cytoscape v.3.9.0. Except
609 where otherwise stated, each experiment in this study was independently repeated
610 three times, and the one-way ANOVA method was used for statistical analysis.

611

612 **Data availability**

613 The raw MS data were deposited in the public ProteomeXchange Consortium via the
614 PRIDE partner repository with the dataset identifier PXD038735 or IPX0005366000
615 (iProx database).

616

617 **Isocitrate dehydrogenase (ICD) enzymatic activity assay**

618 The enzymatic activity of ICD was detected by measuring the amount of NADPH
619 generated by NADP substrate. 10 μg purified ICD or site-specifically Kac ICD protein
620 was mixed with or without 3 μg purified AhCobQ in 180 μL solution buffer (100 mM
621 Tris-HCl, pH 8.0, 0.5 mM NADP, 3 mM $MgCl_2$, 10% glycerol, 1.5 mM isocitrate), and
622 the absorbance of NADPH at OD340nm was detected by SpectraMax® i3(Molecular
623 Devices) once a minute. Simultaneously, serial concentrations of NADPH (0-0.8mM)
624 was incubated with ICD for standard curve determination.

625

626

627

628

629

630

631

632

633

634

635

636

637 ## Figure and Table Legends

638 **Figure 1. Phenotypes of Δ*ahcobB* and Δ*ahcobQ* strains.** (A) Construction
639 of *ahcobB*- and *ahcobQ*-defective strains. M: Marker; Lanes 1 and 3: PCR
640 products of WT using the P7/P8 primer pairs of *ahcobB* and *ahcobQ*,
641 respectively; Lanes 2 and 6: PCR products of *ΔahcobB* and *ΔahcobQ*,
642 respectively, using P7/P8 primer pairs; Lanes 5 and 7: PCR products of WT
643 using P5/P6 primer pairs of *ahcobB* and *ahcobQ*, respectively; Lanes 4 and 8:
644 PCR products of *ΔahcobB* and *ΔahcobQ*, respectively, using the P5/P6 primer
645 pairs. (B) Bacterial migration ability; (C) hemolytic activity; (D) histogram of the
646 biofilm formation ability (OD 595 nm). **P < 0.005.

647

648 **Figure 2. Homology comparison and deacetylase activity assay of**
649 **AhCobQ and AhCobB.** (A) and (B) Homologous and conserved domain
650 analysis of AhCobQ and AhCobB family proteins. (C) and (D) Dot blot and
651 western blot verified the whole cell protein Kac level among WT, Δ*ahcobB*, and
652 Δ*ahcobQ* strains. (E–H) Effect of NAD^+, NAM, Zn^{2+}, and ATP on KDAC
653 enzymatic activity of AhCobQ.

654

655 **Figure 3. Validation of the KDAC activity of AhCobQ by LC-MS/MS.** (A)
656 Retention time of synthetic peptides YNGVFQECCQAEDKGACLLPK (STD)
657 and YNGVFQECCQAEDK^{ac}GACL-L-PK (STD^{*Kac}) with or without AhCobB and
658 AhCoQ treatment; (B) MS1 spectrum of synthetic peptides STD and STD^{*Kac}
659 with or without AhCobB and AhCobQ treatment; (C) and (D) MS2 spectrum of

660 acetylated and unmodified peptides.

661

662 **Figure 4. Lysine deacetylase activity of AhCobQ truncated proteins.**
663 Western blot analysis of the KDAC activity of (A) $AhCobQ_{1–179}$, $AhCobQ_{179–264}$,
664 $AhCobQ_{1–264}$, $AhCobQ_{189–264}$, $AhCobQ_{199–264}$, $AhCobQ_{195–264}$, $AhCobQ_{195–255}$,
665 and $AhCobQ_{200–255}$; (B) $AhCobQ_{179–264}$, $AhCobQ_{189–264}$, $AhCobQ_{189–255}$,
666 $AhCobQ_{189–250}$, $AhCobQ_{189–245}$, and $AhCobQ_{189–240}$ truncated proteins treated
667 with Kac-BSA. The first lane represents Kac-BSA without AhCobQ truncated
668 proteins. The upper part of the figure shows the WB results of the Kac level of
669 truncated proteins with Kac-BSA, and the lower part shows the PVDF
670 membrane R350 staining for the loading amount control. (C) Design of the
671 series of truncated proteins and the summary of the WB results in this
672 experiment. Blue indicates the AAA_31 domain (1–179 aa), and red indicates
673 the unknown range (180–264 aa) in AhCobQ. Black and white indicate the
674 positive and negative WB results, respectively, in this study.

675

676 **Figure 5. Phylogenetic tree of the AhCobQ KDAC activity domain (195–**
677 **245 aa).** Different colors indicate different branches, and *Aeromonas hydrophila*
678 *spp.* is highlighted in red.

679

680 **Figure 6. Proteomics analysis of upregulated proteins in Δ*ahcobB,***
681 **Δ*ahcobQ*, Δ*ahacuC*, and WT strains.** (A) Venn diagrams visualized the
682 overlapped upregulated Kac proteins and Kac peptides among the *Δahcob*B,

683 *ΔahcobQ*, *ΔahacuC*, and WT strains. The number of acetylated proteins and
684 peptides (sites) are shown in the figure. (B) KEGG metabolic pathway
685 enrichment analysis of upregulated Kac proteins and peptides by the three
686 KDACs. Unique and overlapped Kac protein and peptides (sites) are presented
687 in different colors.
688
689 **Figure 7. Western blot validation of the site-specific Kac protein**
690 **substrates regulated by the three KDACs.** (A–C) Kac specific sites were
691 regulated by AhCobQ alone, AhCobQ with AhCobB, and all three KDACs
692 together. The overlapping proteomic features of the target Kac proteins
693 regulated by the three KDACs are shown on the left side of the figure. The
694 detected proteins are in the pink area of the Venn diagram; (D) different Kac
695 sites in one protein substrate were regulated by different KDACs. The predicted
696 3D structure of the target proteins with different Kac sites is shown on the left
697 side of the figure. The middle section shows the WB results of the deacetylation
698 effect of the three KDACs on site-specific Kac protein substrates, and the right
699 shows the PVDF membrane R350 staining for the loading amount control.
700
701 **Figure 8. AhCobQ positively regulates the ICD enzymatic activity through**
702 **deacetylation of K388 on ICD.** (A) western blot verified the deacetylation effect of
703 AhCobQ on ICD and ICD-K388; (B) western blot verified the deacetylation effect of
704 AhCobQ, AhCobB and AhAcuC on ICD-K388. The PVDF membrane R350 staining for
705 the loading amount control was displayed under the WB results; (C) Enzymatic

706 activities of ICD (yellow), ICD-Kac388(blue), ICD-Kac388 treated with AhCobQ (red),
707 ICD-Kac388 treated with AhCobB (green), ICD-Kac388 treated with AhAcuC (brown);
708 (D) The histogram showed the effect of AhCobQ/AhcobB on ICD or ICD-Kac388
709 enzymatic activities at 5min. ***P < 0.001.
710

711 ## Supplementary Figures and Tables

712 **Figure S1. Bacterial swarming ability of Δ*ahcobQ*, WT and *ahcobQ* complement**
713 **strain.**
714

715 **Figure S2. Comparison of homology of AhCobQ protein sequences by using**
716 **BLAST.**
717

718 **Figure S3. Characteristics of overexpressed and purified recombinant proteins**
719 **AhCobQ, AhCobB, and AhAcuC.** (A) PCR amplification results of *ahcobQ*, *ahcobB*,
720 and *ahacuC* gene, respectively; (B) SDS-PAGE gels of purified recombinant proteins
721 AhCobQ, AhCoB, and AhAcuC, respectively. Lane M represents the DNA or protein
722 marker.
723

724 **Figure S4. In vitro acetylated BSA (Kac-BSA) was verified by western blot.**
725

726 **Figure S5. *In vitro* deacetylase activity assay of different recombinant AhCobQ**
727 **proteins in the presence and absence of EDTA utilizing Kac-BSA as substrate.**
728 Purified His-tag (A) and GST-fused (B) recombinant AhCobQ incubated with the

729 substrate Kac-BSA, both with and without EDTA treatment, respectively.

730

731 **Figure S6. The lysine deacetylase activity of AhCobQ didn't be affected by**

732 **0.5mM ATP at different incubation times.**

733

734 **Figure S7. Characteristics of overexpressed and purified recombinant AhCobQ**

735 **truncated proteins.** The PCR amplification and SDS-PAGE results of purified

736 recombinant truncated proteins (GST-fusion) 1: $AhCobQ_{1–179}$; 2: $AhCobQ_{179–265}$; 3:

737 $AhCobQ_{189–265}$; 4: $AhCobQ_{189–255}$; 5: $AhCobQ_{189–250}$; 6: $AhCobQ_{189–245}$; 7: $AhCobQ_{189–240}$;

738 8: $AhCobQ_{195–255}$; 9: $AhCobQ_{200–255}$; 10: $AhCobQ_{179–225}$; 11: $AhCobQ_{179–235}$; 12:

739 $AhCobQ_{179–245}$; 13: $AhCobQ_{179–255}$; 14: $AhCobQ_{189–265}$; 15: $AhCobQ_{199–265}$; 16:

740 $AhCobQ_{209–265}$; 17: $AhCobQ_{219–265}$.

741

742 **Figure S8. Construction of *A. hydrophila ahacuC* knockout mutant strain**

743 M: Marker; Lanes 1 and 2: PCR products of WT and Δ*ahacuC* using the P7/P8 primer

744 pairs; Lanes 3 and 4: PCR products of WT and Δ*ahacuC* using the P5/P6 primer pairs.

745

746 **Figure S9. Scatter plot of Pearson's correlation coefficients of label-free**

747 **quantification (LFQ) intensity among each group and their biological replicates**

748 **in the quantitative acetylome.**

749

750 **Figure S10. Quantitative acetylome analysis among the Δ*ahcobQ*, Δ*ahcobB*,**

751 **Δ*ahacuC*, and WT strains.** Mass error distribution of total identified Kac peptides; (B–

752 D) Volcano plot of the P-values vs. the log2 Kac peptide abundance differences
753 between Δ*ahcobQ* vs. WT, Δ*ahcobB* vs. WT, and Δ*ahacuC* vs. WT, with upregulated
754 Kac proteins outside the significance lines colored in red. Some representative Kac
755 protein names are highlighted.
756
757 **Figure S11. Purified original recombinant proteins (without site-directed**
758 **acetylation modification) without Kac modifications, validated by Western blot.**
759 1: RecA, 2: ADK, 3: FtsA, 4: IscS, 5: HrpA, 6: GyrB, 7: SUN, 8: A0KJ75, 9: ENO, 10:
760 ArcA-2, CK: Kac-BSA, M: prestained protein marker. CK is Kac-BSA as a positive
761 control. The lower section presents the PVDF membrane R350 staining for the loading
762 amount control.
763
764 **Figure S12. Characteristics of the overexpressed and purified recombinant**
765 **target proteins.** The PCR products (right) and SDS-PAGE results of the target
766 recombinant or site-directed acetylated proteins. (A) HrpA and HrpA-K816; (B) SUN,
767 SUN-K103, and SUN-K148; (C) ENO and ENO-K195; (D) ArcA-2 and ArcA-2-K26; (E)
768 ADK and ADK-K48; (F) IscS and IscS-K93; (G) AOKJ75 and AOKJ75-K81; (H) GyrB,
769 GyrB-K331, and GyrB-K449; (I) FtsA, FtsA-K320, and FtsA-K409; (J) RecA, RecA-
770 K279, and RecA-K306; (K) ICD and ICD-K388; (L) GlmM and GlmM-K34.
771
772 **Figure S13. Western blot validated the site-specific Kac protein substrates of**
773 **GlmM-K34 regulated by three KDACs.** The left section shows the WB results of the
774 effect of three KDACs on the GlmM K34 site, and the right section presents the PVDF

775 membrane R350 staining for the loading amount control.

776

777 **Table S1. Selected Kac peptide quantification among Kac-BSA and Kac-**

778 **BSA incubated with CobQ and BSA without acetylation, by LC MS/MS.**

779

780 **Table S2. Acetylation-modified upregulated proteins of AhCobQ-deleted**

781 **strains and the identification of residue positions by LC MS/MS.**

782

783 **Table S3. Chemicals and reagents used in this study.**

784

785 **Table S4. Critical commercial assay kits used in this study.**

786

787 **Table S5. Bacterial strains and plasmids used in this study.**

788

789 **Table S6. Primer pairs used in this study.**

790

791 **Supplementary material 1: Western blot results of the full PVDF membranes from**

792 **this study.**

793

794 **Supplementary material 2. The analysis results of Kac-BSA incubated with**

795 **AhCobQ by LC MS/MS.**

796

797 Figure1.

798

799

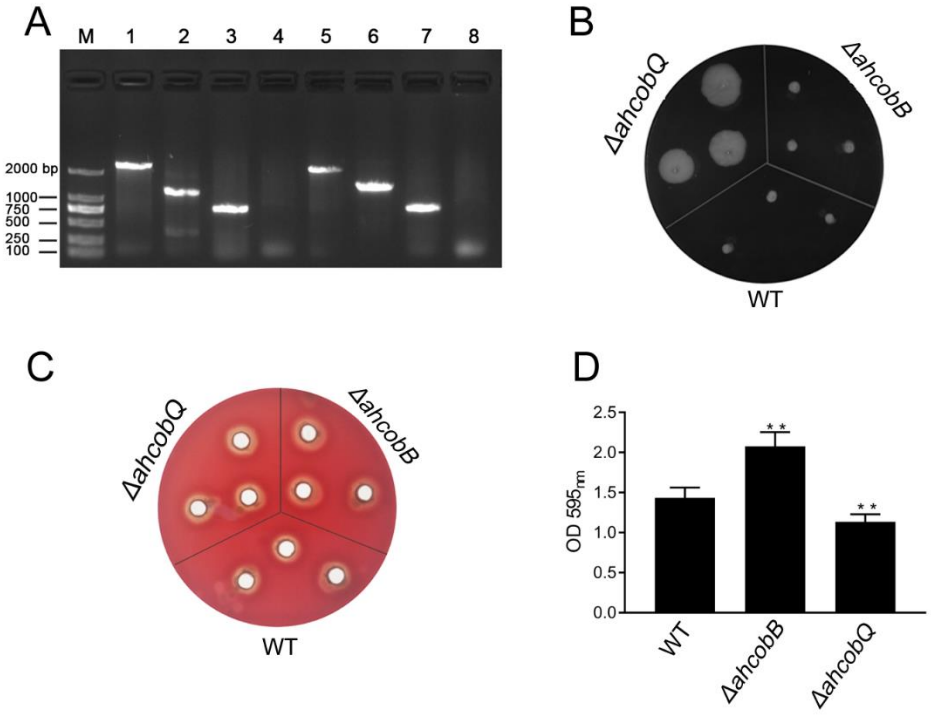

Figure2.

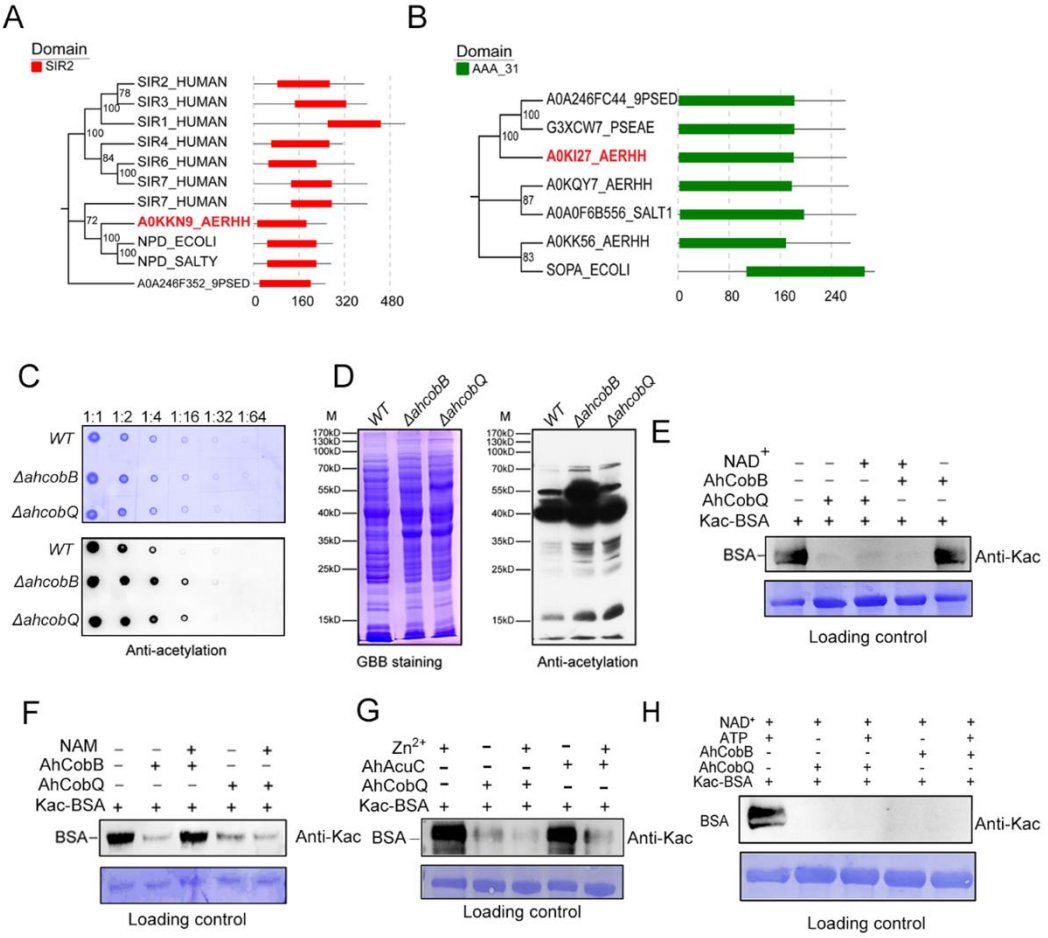
A
Domain
SIR2
SIR2_HUMAN
SIR3_HUMAN
SIR1_HUMAN
SIR4_HUMAN
SIR6_HUMAN
SIR7_HUMAN
SIR7_HUMAN
A0KKN9_AERHH
NPD_ECOLI
NPD_SALTY
A0A246F352_9PSED
0 160 320 480
B
Domain
AAA_31
A0A246FC44_9PSED
G3XCW7_PSEAE
A0KI27_AERHH
A0KQY7_AERHH
A0A0F6B556_SALT1
A0KK56_AERHH
SOPA_ECOLI
0 80 160 240
C
1:1 1:2 1:4 1:16 1:32 1:64
WT
ΔahcobB
ΔahcobQ
Anti-acetylation
D
M
WT
ΔahcobB
ΔahcobQ
GBB staining
Anti-acetylation
E
NAD+
AhCobB
AhCobQ
Kac-BSA
BSA
Anti-Kac
Loading control
F
NAM
AhCobB
AhCobQ
Kac-BSA
BSA
Anti-Kac
Loading control
G
Zn2+
AhAcuC
AhCobQ
Kac-BSA
BSA
Anti-Kac
Loading control
H
NAD+
ATP
AhCobB
AhCobQ
Kac-BSA
BSA
Anti-Kac
Loading control

Figure3.

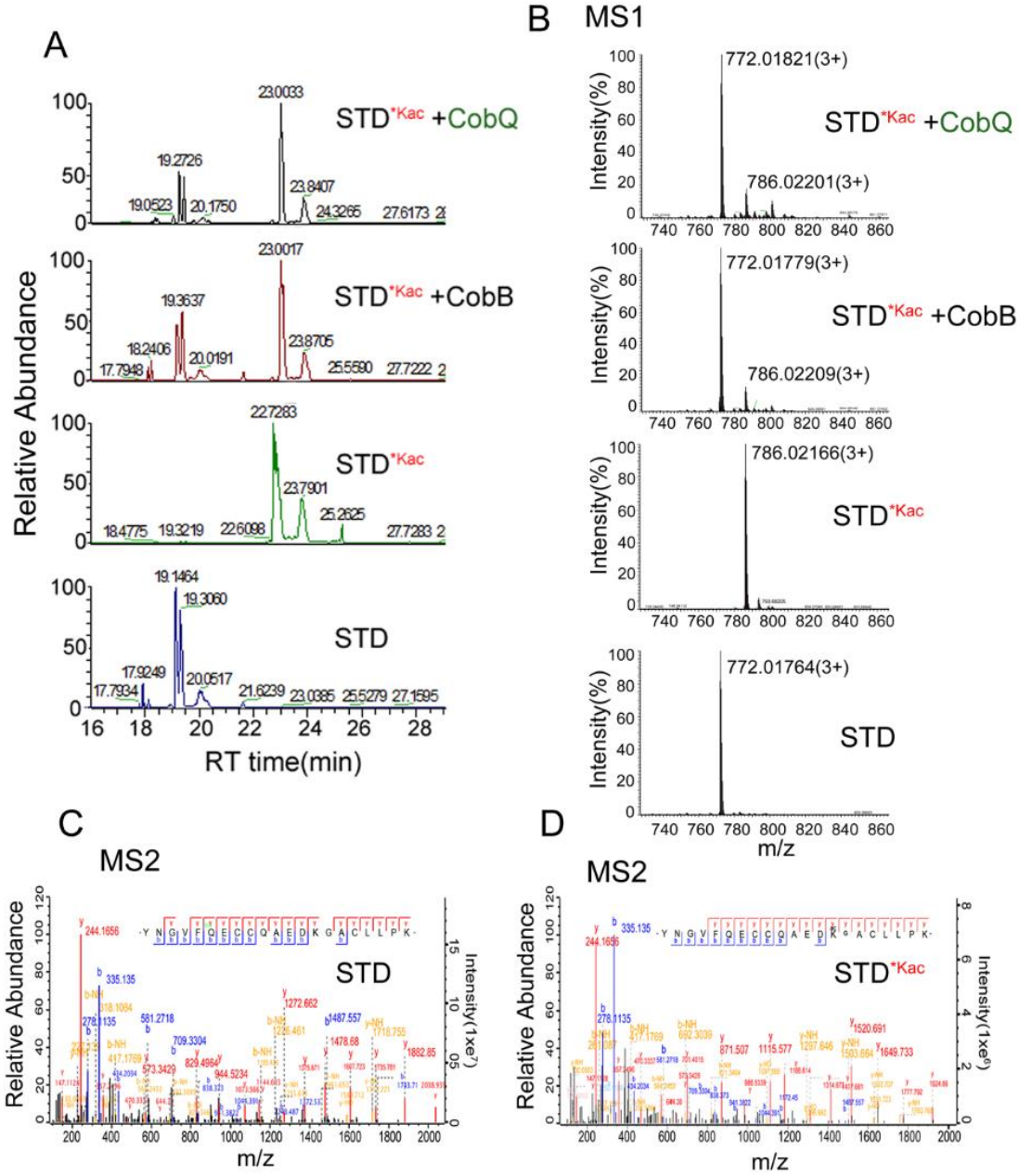
A
STD*Kac +CobQ
STD*Kac +CobB
STD*Kac
STD
Relative Abundance
RT time(min)
B MS1
772.01821(3+)
786.02201(3+)
772.01779(3+)
786.02209(3+)
786.02166(3+)
772.01764(3+)
Intensity(%)
m/z
C
MS2
D
MS2
Relative Abundance
Intensity(1xe7)
Intensity(1xe6)
m/z

808 Figure4.

809

810

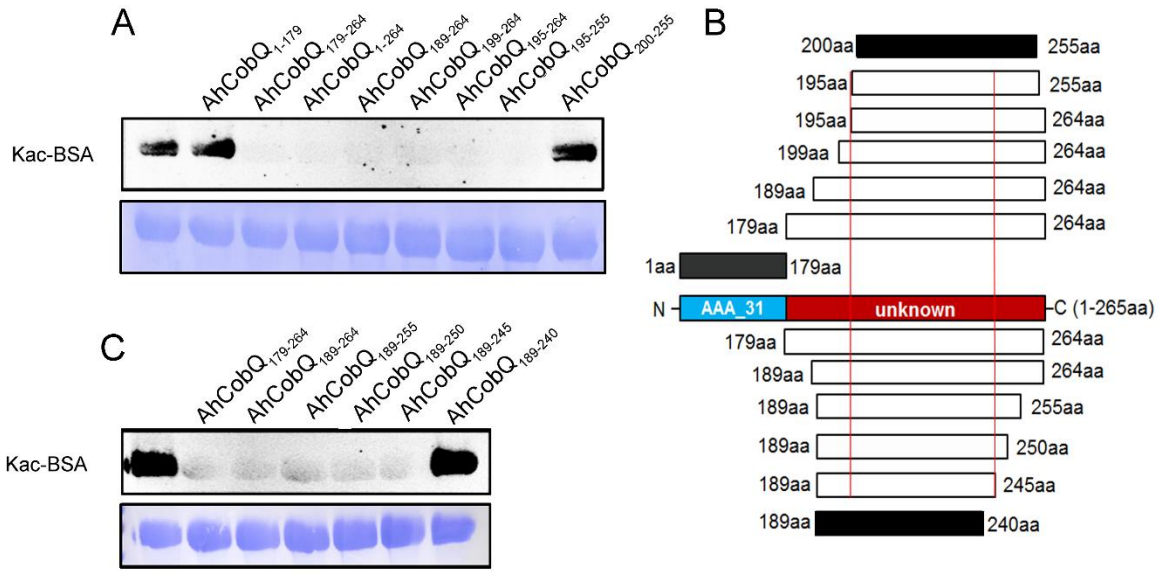

Figure5.

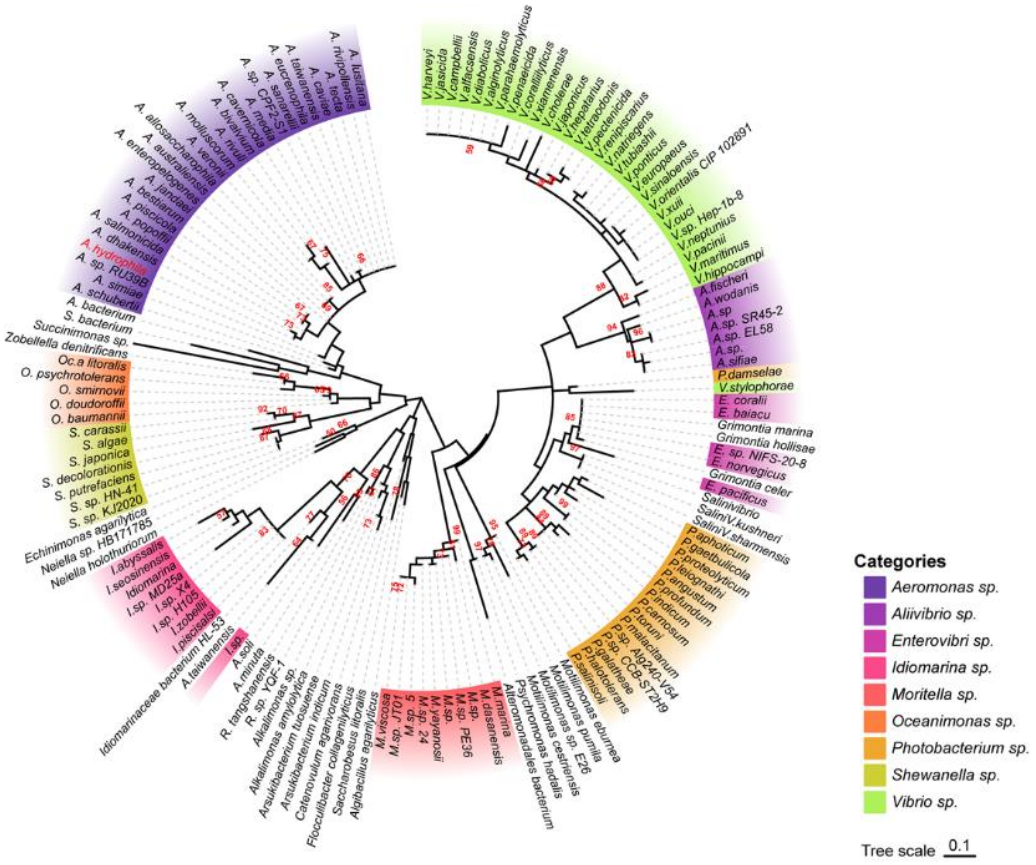
Categories
Aeromonas sp.
Aliivibrio sp.
Enterovibri sp.
Idiomarina sp.
Moritella sp.
Oceanimonas sp.
Photobacterium sp.
Shewanella sp.
Vibrio sp.
Tree scale 0.1

814 Figure6.

815

816

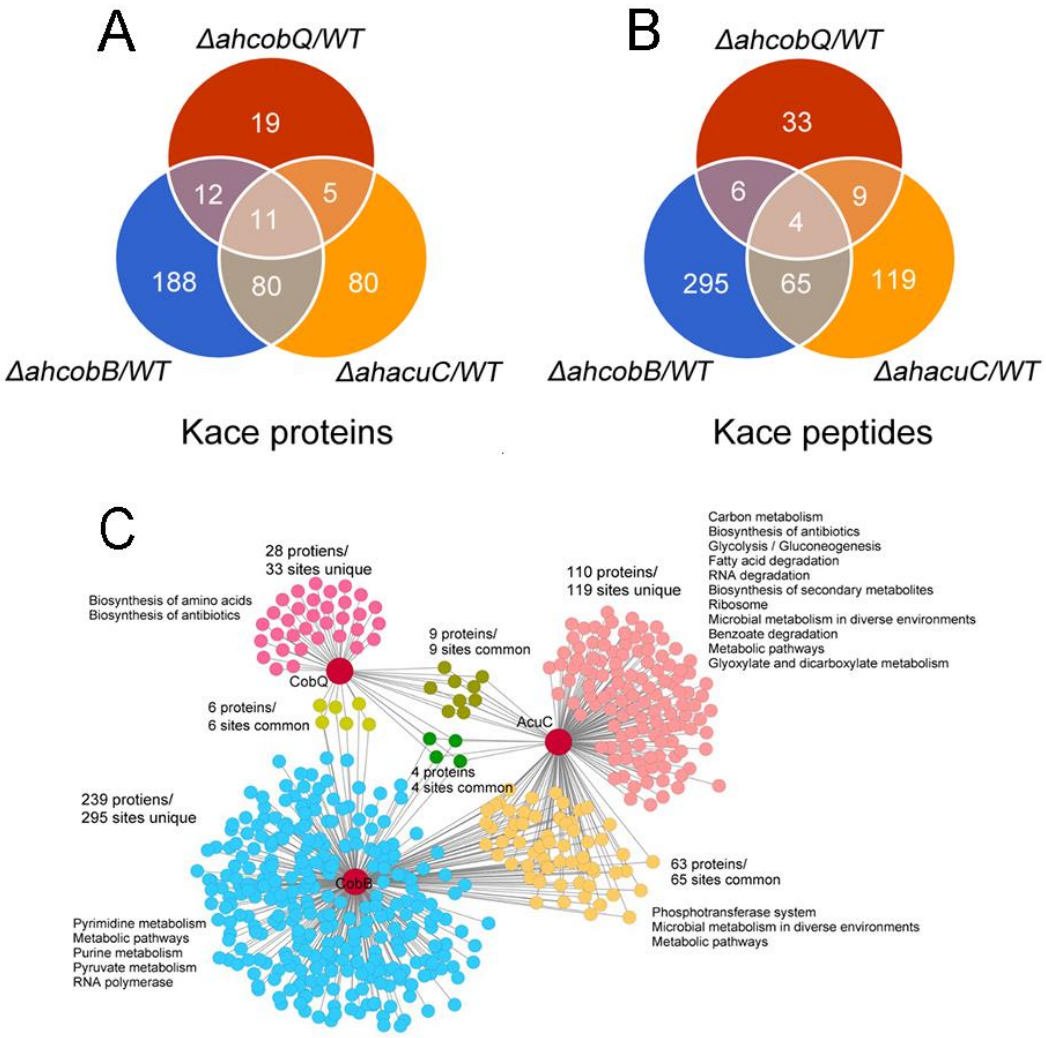

817 Figure7.

818

819

820

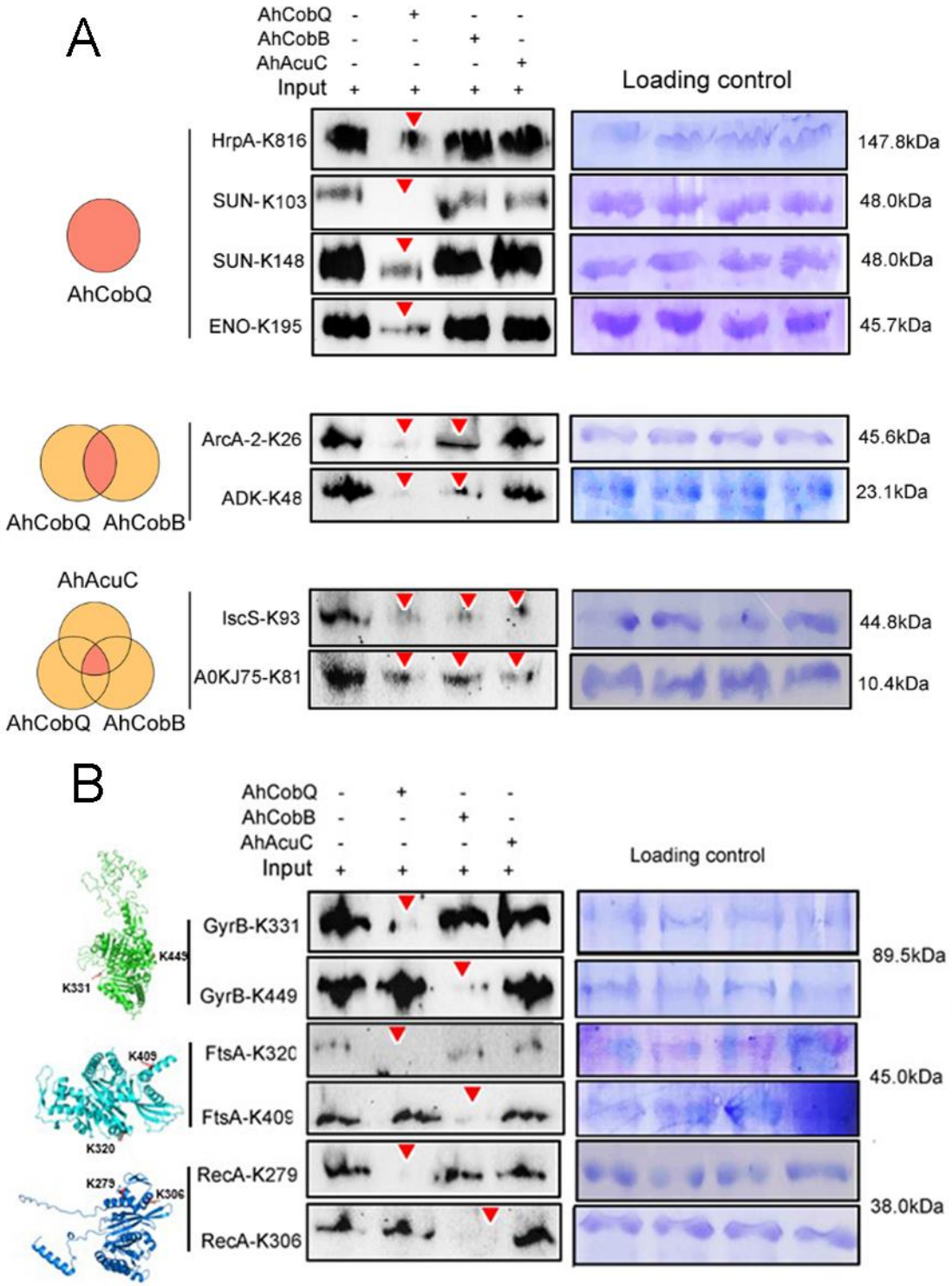

821 Figure8.

822

823

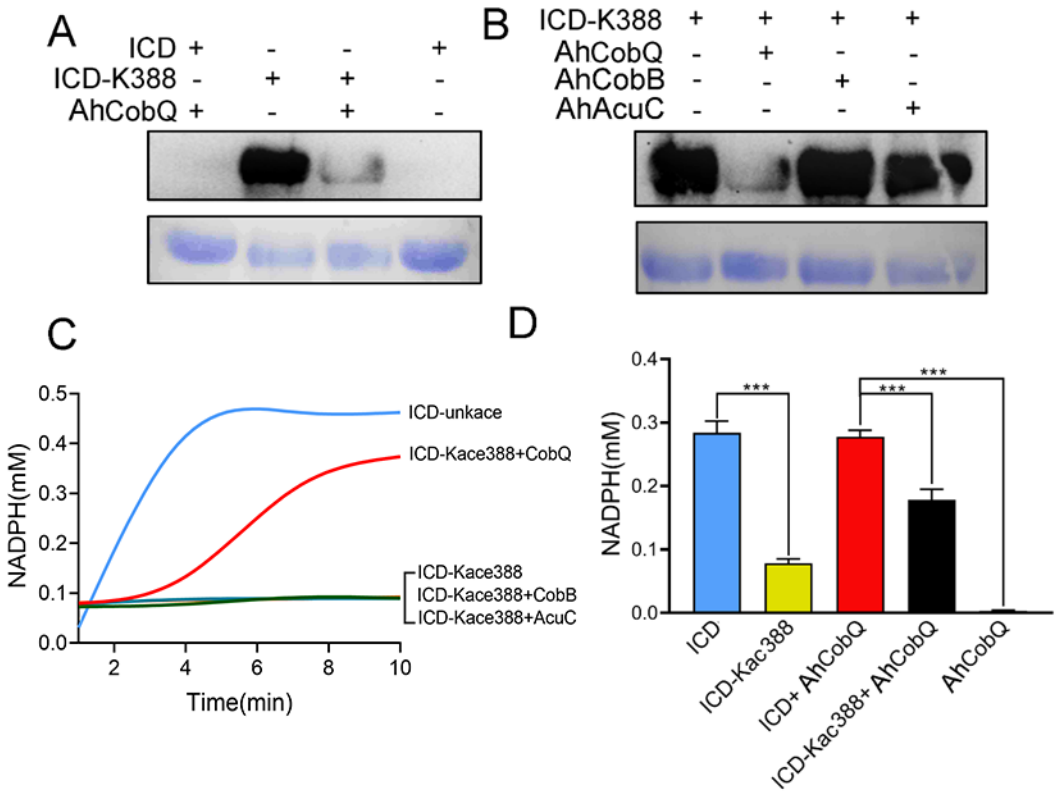

References

AbouElfetouh A, Kuhn ML, Hu LI, Scholle MD, Sorensen DJ, Sahu AK, Becher D, Antelmann H, Mrksich M, and Anderson WF (2015). The *E. coli* sirtuin CobB shows no preference for enzymatic and nonenzymatic lysine acetylation substrate sites. *Microbiology* 4, 66-83.

Brino L, Urzhumtsev A, Mousli M, Bronner C, Mitschler A, Oudet P, and Moras D (2000). Dimerization of *Escherichia coli* DNA-gyrase B provides a structural mechanism for activating the ATPase catalytic center. *J. Biol. Chem.* 275, 9468-9475.

Bryson D I, Fan C, Guo LT, Miller C, Söll D, and Liu DR (2017). Continuous directed evolution of aminoacyl-tRNA synthetases. *Nat. Chem. Biol.*13, 1253-1260.

Burckhardt RM, Buckner BA, and Escalante-Semerena JC (2019). *Staphylococcus aureus* modulates the activity of acetyl-Coenzyme A synthetase (Acs) by sirtuin-dependent reversible lysine acetylation. *Mol. Microbiol.*112, 588-604.

Cai Q, Wang G, Li Z, Zhang L, Fu Y, Yang X, Lin W, and Lin X (2019). SWATH based quantitative proteomics analysis reveals Hfq2 play an important role on pleiotropic physiological functions in *Aeromonas hydrophila. J. Proteomics.* 195, 1-10.

Carabetta VJ, Greco TM, Cristea IM, Dubnau D (2019). YfmK is an Nε-lysine acetyltransferase that directly acetylates the histone-like protein HBsu in *Bacillus subtilis*. *PNAS.*116, 3752-3757.

Chauffour A, Morel F, Reibel F, Petrella S, Mayer C, Cambau E, and Aubry A (2021). A systematic review of *Mycobacterium leprae* DNA gyrase mutations and their impact on fluoroquinolone resistance. *Clin. Microbiol. Infec.*27, 1601-1612.

Chen X, Ding AB, and Zhong X (2020). Functions and mechanisms of plant histone deacetylases. Sci. China. *Life. Sci.*63, 206-216.

Chen YJC, Koutelou E, and Dent SY (2022). Now open: evolving insights to the roles of lysine acetylation in chromatin organization and function. *Mol. Cell.* 82, 716-727.

Galperin MY, and Grishin NV (2000). The synthetase domains of cobalamin biosynthesis amidotransferases *cobB* and *cobQ* belong to a new family of ATP-dependent amidoligases, related to dethiobiotin synthetase. *Proteins.* 41, 238-247.

Guan KL, Yu W, Lin Y, Xiong Y, and Zhao S (2010). Generation of acetyllysine antibodies and affinity enrichment of acetylated peptides. *Nat. Protoc.*5, 1583-1595.

Hor, Z. N., Mohamad, M. S., Choon, Y. W., Remli, M. A., & Majid, H. A. (2024). A Hybrid of Differential Evolution and Minimization of Metabolic Adjustment for Succinic and Ethanol Production. *BAIDAMS*, 205-217.

Huang S, Zhao J, Li W, Wang P, Xue Z, and Zhu G (2021). Biochemical and phylogenetic characterization of a novel NADP+-specific isocitrate dehydrogenase from the marine microalga *Phaeodactylum tricornutum*. *Front. Mol. Biosci.*8, 702083.

Hwang CS, Shemorry A, and Varshavsky A (2010). N-terminal acetylation of cellular proteins creates specific degradation signals. *Science* 327, 973-977.

Jiang M, Chen ZG, Li H, Zhang TT, Yang MJ, Peng XX, and Peng B (2022). Succinate and inosine coordinate innate immune response to bacterial infection. *PLoS Pathog* 18, e1010796.

Kou TS, Wu JH, Chen XW, Chen ZG, Zheng J, and Peng B (2022). Exogenous glycine promotes oxidation of glutathione and restores sensitivity of bacterial pathogens to serum-induced cell death. *Redox Biol.* 58, 102512.

Kuhn ML, Zemaitaitis B, Hu LI, Sahu A, Sorensen D, Minasov G, Lima BP, Scholle M, Mrksich M, and Anderson WF (2014). Structural, kinetic and proteomic characterization of acetyl phosphate-

dependent bacterial protein acetylation. *PloS one* 9, e94816.
Li L, Yang B, Wang J, Wei Y, Xiang B, Liu Y, Wu P, Li W, Wang Y, Zhao X, Qin J (2024). CobB-mediated deacetylation of the chaperone CesA regulates *Escherichia coli* O157: H7 virulence. *Gut Micro*. 16, 2331435.
Li J, Wei Y, Wang J, Li Y, Shao G, Feng Z, and Xiong Q (2022). Characterization of mutations in DNA gyrase and topoisomerase IV in field strains and in vitro selected quinolone-resistant *Mycoplasma hyorhinis* mutants. *Antibiotics-basel* 11, 494.
Li Z, Wang Y, Li X, Lin Z, Lin Y, Srinivasan R, and Lin X (2019). The characteristics of antibiotic resistance and phenotypes in 29 outer-membrane protein mutant strains in *Aeromonas hydrophila*. *Environ. Microbiol*. 21, 4614-4628.
Liu W, Tan Y, Cao S, Zhao H, Fang H, Yang X, Wang T, Zhou Y, Yan Y, and Han Y (2018). Protein acetylation mediated by YfiQ and CobB is involved in the virulence and stress response of *Yersinia pestis*. *Infect. Immun*. 86, 00224-00218.
Macek B, Forchhammer K, Hardouin J, WeberBan E, Grangeasse C, and Mijakovic I (2019). Protein post-translational modifications in bacteria. *Nat. Rev. Microbiol.* 17, 651-664.
Mou X, Spinard EJ, Hillman SL, and Nelson DR (2017). Isocitrate dehydrogenase mutation in *Vibrio anguillarum* results in virulence attenuation and immunoprotection in rainbow trout (Oncorhynchus mykiss). *BMC Microbiol.* 17, 1-14.
Narita T, Weinert BT, and Choudhary C (2019). Functions and mechanisms of non-histone protein acetylation. Nat. Rev. *Mol. Cell Bio.*20, 156-174.
Pang HY, Li WX, Zhang W, Zhou S, Hoare R, Monaghan SJ, Jian JC, and Lin XM (2020). Acetylome profiling of *Vibrio alginolyticus* reveals its role in bacterial virulence. *J. Proteomics* 211, 103543.
Peng BO, Su YB, Li H, Han YI, Guo C, Tian YM and Peng XX (2019). Exogenous alanine and/or glucose plus kanamycin kills antibiotic-resistant bacteria. *Cell Metab* 21, 249-262.
Rajendran A, Soory A, Khandelwal N, Ratnaparkhi G, and Kamat SS (2022). A multi-omics analysis reveals that the lysine deacetylase ABHD14B influences glucose metabolism in mammals. *J. Biol. Chem.*298.
Rajendran A, Vaidya K, Mendoza J, BridwellRabb J, and Kamat SS (2019). Functional annotation of ABHD14B, an orphan serine hydrolase enzyme. *Biochem*. 59, 183-196.
Schilling B, Christensen D, Davis R, Sahu AK, Hu LI, WalkerPeddakotla, A, Sorensen, DJ, Zemaitaitis, B, Gibson, BW, and Wolfe, AJ (2015). Protein acetylation dynamics in response to carbon overflow in *E scherichia coli*. *Mol. Microbiol.*98, 847-863.
Seshadri R, Joseph SW, Chopra AK, Sha J, Shaw J, Graf J, Haft D, Wu M, Ren Q, and Rosovitz M. (2006). Genome sequence of *Aeromonas hydrophila* ATCC 7966T: jack of all trades. *J. Bacteriol.*188, 8272-8282.
Sun L, Yao Z, Guo Z, Zhang L, Wang Y, Mao R, Lin Y, Fu Y, and Lin X (2019). Comprehensive analysis of the lysine acetylome in *Aeromonas hydrophila* reveals cross-talk between lysine acetylation and succinylation in LuxS. *Emerg. Microbes Infect.* 8, 1229-1239.
Tari LW, Trzoss M, Bensen DC, Li X, Chen Z, Lam T, Zhang J, Creighton CJ, Cunningham M.L., and Kwan B. (2013). Pyrrolopyrimidine inhibitors of DNA gyrase B (GyrB) and topoisomerase IV (ParE). Part I: Structure guided discovery and optimization of dual targeting agents with potent, broad-spectrum enzymatic activity. *Bioorg Med. Chem.* Lett.23, 1529-1536.
Tsang AW, and EscalanteSemerena JC (1998). CobB, a new member of the SIR2 family of eucaryotic regulatory proteins, is required to compensate for the lack of nicotinate mononucleotide: 5, 6-

912 dimethylbenzimidazole phosphoribosyltransferase activity in cobT mutants during cobalamin
913 biosynthesis in *Salmonella typhimurium* LT2. J. *Biol. Chem.*273, 31788-31794.
914 VanDrisse CM, and EscalanteSemerena JC (2019). Protein acetylation in bacteria. *Annu. Rev.*
915 *Microbiol.*73, 111-132.
916 Venkat S, Chen H, Stahman A, Hudson D, McGuire P, Gan Q, and Fan C (2018). Characterizing
917 lysine acetylation of isocitrate dehydrogenase in *Escherichia coli. J. Mol. Biol.*430, 1901-1911.
918 Vidali G, Gershey E, and Allfrey V (1968). Chemical Studies of Histone Acetylation: The distribution
919 of ε-N-acetyllysine in calf thymus histones. *J. Biol. Chem.*243, 6361-6366.
920 Wang G, Wang Y, Zhang L, Cai Q, Lin Y, Lin L, and Lin X (2020). Proteomics analysis reveals the
921 effect of *Aeromonas hydrophila* sirtuin CobB on biological functions. *J. Proteomics.* 225, 103848.
922 Wang Q, Zhang Y, Yang C, Xiong H, Lin Y, Yao J, Li H, Xie L, Zhao W, and Yao Y (2010). Acetylation
923 of metabolic enzymes coordinates carbon source utilization and metabolic flux. *Science* 327,
924 1004-1007.
925 Wang ZA, and Cole PA (2020). The chemical biology of reversible lysine post-translational
926 modifications. *Cell Chem. Biol.*27, 953-969.
927 Watson PR, and Christianson DW (2023). Structure and Function of Kdac1, a class II deacetylase
928 from the multidrug-resistant pathogen *Acinetobacter baumannii. Biochem* 62, 2689-2699.
929 Weinert BT, Iesmantavicius V, Wagner SA, Schölz C, Gummesson B, Beli P, Nyström T, and
930 Choudhary C. (2013). Acetyl-phosphate is a critical determinant of lysine acetylation in *E. coli. Mol.*
931 *Cell* 51, 265-272.
932 Weinert BT, Satpathy S, Hansen BK, Lyon D, Jensen LJ, and Choudhary C. (2017). Accurate
933 quantification of site-specific acetylation stoichiometry reveals the impact of sirtuin deacetylase
934 CobB on the *E. coli* acetylome. *Mol. Cell. Proteomics.*16, 759-769.
935 Witze ES, Old WM, Resing KA, and Ahn N.G. (2007). Mapping protein post-translational
936 modifications with mass spectrometry. *Nat. Methods.*4, 798-806.
937 Yoshida M, Kudo N, Kosono S, and Ito A (2017). Chemical and structural biology of protein lysine
938 deacetylases. *P. Jpn. Acad.Series B* 93, 297-321.
939 Yu K, Wang Y, Zheng Y, Liu Z, Zhang Q, Wang S, Zhao Q, Zhang X, Li X, and Xu RH (2023). qPTM:
940 an updated database for PTM dynamics in human, mouse, rat and yeast. *Nucleic. Acids.Res.* 51,
941 D479-D487.
942 Zhang L, Yao Z, Tang H, Song Q, Song H, Yao J, Li Z, Xie X, Lin Y, and Lin X (2022). The lysine
943 acetylation modification in the porin Aha1 of *Aeromonas hydrophila* regulates the uptake of
944 multidrug antibiotics. *Mol. Cell. Proteomics.* 21, 100248.
945 Zhao L, Liu Q, Huang Q, Liu F, Liu H, and Wang G (2021). Isocitrate dehydrogenase of *Bacillus*
946 *cereus* is involved in biofilm formation. *World J. Microb. Biot.*37, 207.
947

948

Acknowledgments

This work was supported by grants from Key projects of National Natural Science Foundation of China (NSFC) (32171435, 32001045), Natural Science Foundation of Fujian Province (2020J02023), Key Laboratory of Marine Biotechnology of Fujian Province (2020MB04), Natural Science Foundation of Fujian Province (2018J01598), Program for Innovative Research Team in Fujian Agricultural and Forestry University (712018009), and the Fujian-Taiwan Joint Innovative Center for Germplasm Resources and Cultivation of Crop (FJ 2011 Program, 2015-75,). We thank the help from Central Laboratory, Fujian Medical University Union Hospital, PR China, and LetPub (www.letpub.com) for its linguistic assistance during the preparation of this manuscript.

Author contributions

Yuqian Wang and Guibin Wang conceptualized and validated the study. Lishan Zhang performed the methodology and the data curation and wrote the manuscript for the final draft. Qilan Cai, Meizhen Lin, Dongping Huang and Yuyue Xie performed the formal analysis. Wenxiong Lin and Xiangmin Lin was responsible for the resources, supervised the study, and performed the funding acquisition. Yuqian Wang, Guibin Wang and Xiangmin Lin wrote, reviewed, and edited the manuscript. All authors contributed to the article and approved the submitted version.

Competing interests

971 The authors declare no competing interests.